Full-Duplex GFDM Radio Transceivers in the Presence of Phase Noise, CFO and IQ Imbalance

Amirhossein Mohammadian, *Student Member, IEEE*, and Chintha Tellambura, *Fellow, IEEE*
Department of Electrical and Computer Engineering University of Alberta, Edmonton, Alberta, Canada
Email: am11@ualberta.ca and chintha@ece.ualberta.ca

***Abstract*—This paper addresses the performance of a full-duplex (FD) generalized frequency division multiplexing (GFDM) transceiver in the presence of radio frequency (RF) impairments including phase noise, carrier frequency offset (CFO) and in-phase (I) and quadrature (Q) imbalance. We study analog and digital self-interference (SI) cancellation and develop a complementary SI suppression method. Closed-form solutions for the residual SI power and the desired signal power and signal-to-interference ratio (SIR) are provided. Simulation results show that the RF impairments degrade SI cancellation and FD GFDM is more sensitive to them compares to FD orthogonal frequency division multiplexing (OFDM). Hence, we propose an FD GFDM receiver filter for maximizing the SIR. Significantly, it achieves 25 dB higher SIR than FD OFDM transceiver.**

***Index Terms*—Full-duplex radios, generalized frequency division multiplexing (GFDM), radio frequency (RF) impairments, signal-to-interference ratio (SIR), filter design.**

I. Introduction

Due to the increasing wireless data and emerging fifth generation (5G) networks, full-duplex (FD) radio may be the answer to handle higher capacity demands [1], [2]. FD radios can simultaneously transmit and receive on the same frequency and time slots, which potentially doubles the capacity, reduces network delay, improves network secrecy and increases spectrum usage flexibility [2], [3]. Applications of FD wireless are numerous (see [4] and [5] and references therein). Moreover, 4G wireless cellular deploys orthogonal frequency division multiplexing (OFDM), which may not be sufficient to reach all vital requirements of 5G. A potential alternative to OFDM is generalized frequency division multiplexing (GFDM), a filtered multicarrier modulation scheme with low out-of-band (OOB) emissions, high spectral efficiency and low latency [6], [7]. Thus, the combination of GFDM and FD may be the ideal architecture to achieve 5G network requirements.

The fundamental challenge in the FD radios is the self-interference (SI) due to the coupling of the transmit signal to the receiver path during simultaneous transmission and reception. To mitigate SI, active cancellation is performed over the analog and digital parts of the receiver chain [8]. In the analog part, the dominant SI component is suppressed by subtracting adjusted transmitted signal in amplitude, time and phase from the received signal. The rest of the multipath components are processed in digital part by estimating the channel-state information (CSI). However, in direct conversion transceivers, radio frequency (RF) impairments in front-end components including phase noise, carrier frequency offset (CFO) and in-phase (I) and quadrature (Q) imbalance degrade the link performance significantly. In the FD system, these RF imperfections will limit the capability of the SI cancellation mechanisms, which must be carefully considered when evaluating the system performance.

In [9], the authors investigate the harmful effects of phase noise on the SI cancellation capability of an FD OFDM transceiver and observe that phase noise limits the performance of the SI suppression techniques. The same transceiver under nonlinear power amplifier and IQ imbalance is studied in [10]. It is shown that IQ imbalance adds image components to the SI signal which have detrimental effects on SI cancellation. Moreover, in [11], phase noise and IQ imbalance in an FD OFDM transceiver are investigated. A scheme for estimation and cancellation the effects of the IQ imbalance, power amplifier nonlinearity and phase noise on an FD OFDM transceiver is proposed in [12]. For the GFDM waveform, impacts of timing offset, CFO and phase noise are studied in [13]. Optimal filter design for a GFDM transceiver in presence of CFO is presented in [14]. GFDM performance in cognitive radio is studied in [15], [16] and effects of the nonlinear power amplifier are investigated for that. Digital interference cancellation scheme for an FD GFDM transceiver is proposed in [17] and SI power is calculated as well. Analog cancellation which suppresses the dominant part of SI power is not considered in [17] and the effects of the RF impairments are not analyzed. Furthermore, to our best knowledge, the FD GFDM transceiver has not been properly modeled with analog and digital SI cancellation and impacts of the phase noise, CFO and IQ imbalance have not been studied. In this paper, we study the FD GFDM transceiver performance in presence of the phase noise, CFO and IQ imbalance.

In detail, the contributions of this paper are as follows:

- We fully model the FD GFDM transceiver by considering the phase noise, CFO and IQ imbalance. Both analog and digital SI cancellation stages are addressed and a complementary method for more suppression of the SI signal in digital domain is developed.
- Residual SI power after analog and digital SI cancellations is derived. Moreover, power of the intended signal in presence of the RF impairments in the receiver is presented. To the best of our knowledge, the collective impact of phase noise, CFO and IQ imbalance has not been investigated for GFDM half-duplex (HF) transceivers, which we do in this paper.

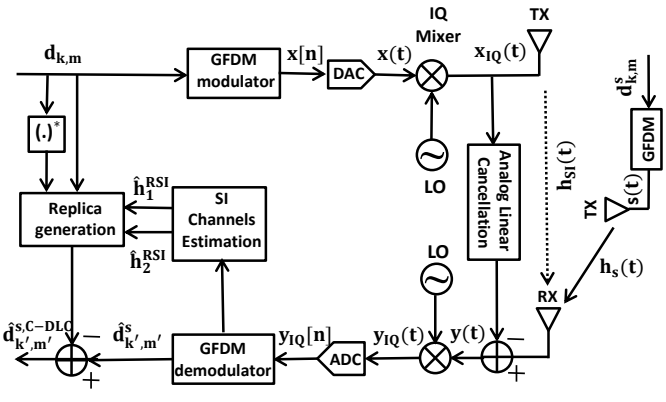

Fig. 1: FD GFDM transceiver.

- By utilizing the derived signal, signal-to-interference ratio (SIR) for received signal is derived. Based on our analysis, we find that FD GFDM is more sensitive to the RF impairments compared to FD OFDM. To mitigate this problem, we design an optimal FD-GFDM receiver filter to maximize the SIR.
- All the theoretical derivations are verified with simulation results. Moreover, to determine the performance gains of FD GFDM transceiver, we also present FD OFDM transceiver results.

II. System Model

The signal model of FD GFDM transceiver in presence of RF impairments including phase noise, CFO and IQ imbalance is shown in Fig. 1. The transmitter and the receiver deploy single separate antennas and the well-known direct-conversion architecture. The SI cancellation relies on analog linear cancellation (ALC) in first stage of the receiver and digital linear cancellation (DLC) in baseband unit. In following, we model and analyze the system in detail.

The GFDM transmitter generates the signal in which data of M-th time-slots are transmitted on the K-th subcarriers. For one symbol time, the GFDM signal may be expressed as

$$x[n] = \sum_{k=0}^{K-1} \sum_{m=0}^{M-1} d_{k,m} g_m[n] e^{\frac{j2\pi kn}{K}}, \quad 0 \le n \le MK-1 \tag{1}$$

where $d_{k,m}$ is zero mean independent and identically distributed (i.i.d.) complex data symbol on k-th subcarrier of m-th time-slot with symbol energy P_d and $g_m[n] = g[n - mK]_{MK}$ is a circularly shifted version of normalized prototype filter $g[n]$ ($\sum_{n=0}^{MK-1} |g[n]|^2 = 1$). With the addition of cyclic prefix (CP) and passing through digital-to-analog conversion (DAC), the analog baseband signal, $x(t)$, is passed through IQ mixer. Due to mismatches between the amplitudes and phases of I-and Q-branches, an undesired signal, which is the mirror image of the original signal, is added. Thus, the output signal of the IQ mixer may be written as

$$x_{IQ}(t) = (g_{Tx,d} x(t) + g_{Tx,I} x^*(t)) e^{j\phi_{Tx}(t)} \tag{2}$$

where $(.)^*$ indicates complex conjugate, $g_{Tx,d}$ and $g_{Tx,I}$ are the transmitter IQ mixer responses for the direct and image signals, respectively, and $\phi_{Tx}(t)$ is random phase noise of the local oscillator of the transmitter side. After passing the transmitter signal through wireless channel and applying ALC, the received signal could be formulated as

$$y(t) = s(t) * h_s(t) + x_{IQ}(t) * h_{RSI}(t) + w(t) \tag{3}$$

where $*$ denotes the convolution, $s(t)$ is desired signal, $h_s(t)$ is multipath desired channel from the intended transmitter to the local receiver, $h_{RSI}(t) = h_{SI}(t) - h_{ALC}(t)$ is residual SI channel where $h_{ALC}(t)$ is estimate of the the multipath coupling channel and $h_{SI}(t)$ is the multipath coupling channel between the local transmitter and the receiver, and $w(t)$ is a Gaussian noise. Then, the signal goes through the receiver IQ mixer which the output is written as

$$y_{IQ}(t) = g_{Rx,d} y(t) e^{-j\phi_{Rx}(t)} e^{j2\pi\Delta_f t} + g_{Rx,I} y^*(t) e^{j\phi_{Rx}(t)} e^{-j2\pi\Delta_f t} \tag{4}$$

where $g_{Rx,d}$ and $g_{Rx,I}$ are the receiver IQ mixer responses for the direct and image signals. $\phi_{Rx}(t)$ is random phase noise of the local oscillator of the receiver side and Δ_f indicates the difference between carrier frequency of the receiver and transmitter local oscillators. Image rejection ratio (IRR) is considered for quantifying the quality of the IQ mixer which is defined as $\text{IRR}_{Rx} = \frac{|g_{Rx,I}|^2}{|g_{Rx,d}|^2}$. By assuming L-tap propagation channels ($h[n] = \sum_{l=0}^{L-1} h_l \delta[n-l]$), according to (2), (3) and (4), the discrete sample of the signal could be expressed as

$$\begin{aligned} y_{IQ}[n] = \sum_{l=0}^{L-1} & h_1^{RSI}[n,l] x[n-l] + h_2^{RSI}[n,l] x^*[n-l] + \\ & h_1^s[n,l] s[n-l] + h_2^s[n,l] s^*[n-l] + w_d[n] + w_I[n] \end{aligned} \tag{5}$$

where equivalent channel responses for individual signal components can be written as

$$\begin{aligned} h_1^{RSI}[n,l] =& g_{Tx,d} g_{Rx,d} h_{RSI,l} e^{j(\phi_{TX}[n-l] - \phi_{RX}[n])} e^{\frac{j2\pi\epsilon n}{K}} + \\ & g_{Tx,I}^* g_{Rx,I} h_{RSI,l}^* e^{-j(\phi_{TX}[n-l] - \phi_{RX}[n])} e^{\frac{-j2\pi\epsilon n}{K}} \\ h_2^{RSI}[n,l] =& g_{Tx,I} g_{Rx,d} h_{RSI,l} e^{j(\phi_{TX}[n-l] - \phi_{RX}[n])} e^{\frac{j2\pi\epsilon n}{K}} + \\ & g_{Tx,d}^* g_{Rx,I} h_{RSI,l}^* e^{-j(\phi_{TX}[n-l] - \phi_{RX}[n])} e^{\frac{-j2\pi\epsilon n}{K}} \\ h_1^s[n,l] =& g_{Rx,d} h_{s,l} e^{-j\phi_{RX}[n]} e^{\frac{j2\pi\epsilon n}{K}} \\ h_2^s[n,l] =& g_{Rx,I} h_{s,l}^* e^{j\phi_{RX}[n]} e^{\frac{-j2\pi\epsilon n}{K}} \\ w_d[n] =& g_{Rx,d} e^{-j\phi_{RX}[n]} e^{\frac{j2\pi\epsilon n}{K}} w[n] \\ w_d[n] =& g_{Rx,I} e^{j\phi_{RX}[n]} e^{\frac{-j2\pi\epsilon n}{K}} w^*[n] \end{aligned} \tag{6}$$

where ϵ is normalized CFO. At the digital domain before deploying DLC, samples are sent to GFDM demodulator where the estimated symbol at k'-th subcarrier and m'-th time-slot is

$$\widehat{d}^s_{k',m'} = \sum_{n=0}^{MK-1} (y_{IQ}[n]) f_{m'}[n] e^{\frac{-j2\pi k' n}{K}} \tag{7}$$

where $f_m[n] = f[n - mK]_{MK}$ is circularly shifted version of receiver filter impulse response $f[n]$. Finally, to further decrease the residual SI signal, by utilizing the replica of transmitted symbols and estimation of the equivalent residual SI channels, digital cancellation symbols are generated and subtracted from the demodulated symbols which is named by classical DLC. Furthermore, [10] shows that after the classical DLC, the image of the SI signal is the dominant source of distortion. Thus, complementary DLC (C-DLC) is proposed in which the cancellation of the image of SI signal is done similar to classical DLC by deploying the conjugate of the transmitted symbols. The output of C-DLC could be expressed as

$$\begin{aligned}\widehat{d}^{s,C-DLC}_{k',m'} = \left(R^{SI}_{k',m'} - R^{DLC}_{k',m'}\right) + \left(R^{SI,im}_{k',m'} - R^{DLC,i}_{k',m'}\right) + \\ R^{s}_{k',m'} + R^{s,im}_{k',m'} + w^{eq}_{k',m'} + w^{eq,im}_{k',m'}\end{aligned} \tag{8}$$

where $R^{SI}_{k',m'}$, $R^{SI,im}_{k',m'}$, $R^{s}_{k',m'}$, $R^{s,im}_{k',m'}$, $w^{eq}_{k',m'}$ and $w^{eq,im}_{k',m'}$ are corresponding terms for SI signal, intended signal and the equivalent noise after GFDM demodulator that are derived from (1) and (5)-(7). Moreover, $R^{DLC}_{k',m'}$ and $R^{DLC,i}_{k',m'}$ are DLC terms for linear and conjugate replica of the symbol, which are written as

$$\begin{aligned}R^{DLC}_{k',m'} &= d_{k',m'} \sum_{l=0}^{L-1}\sum_{n=0}^{MK-1} \hat{h}_1^{RSI}[n,l] f_{m'}[n] g_{m'}[n-l] e^{\frac{-j2\pi k' l}{K}} \\ R^{DLC,i}_{k',m'} &= d^*_{k',m'} \sum_{l=0}^{L-1}\sum_{n=0}^{MK-1} \hat{h}_2^{RSI}[n,l] f_{m'}[n] g^*_{m'}[n-l] e^{\frac{-j2\pi k' (2n-l)}{K}}\end{aligned} \tag{9}$$

where $\hat{h}_1^{RSI}[n,l]$ and $\hat{h}_2^{RSI}[n,l]$ indicate equivalent channel estimation of the linear SI signal and the conjugate SI signal, respectively. It is worth mentioning that output of the classical DLC is derived by, $\widehat{d}^{s,DLC}_{k',m'} = \widehat{d}^{s,C-DLC}_{k',m'} + R^{DLC,i}_{k',m'}$

III. Signal power analysis

In this section, we calculate the power of the residual SI signal and the desired signal in closed-form. The channels, transmitted data and phase noise are assumed as independent random processes. Furthermore, perfect channel estimation and two independent oscillators for the local transmitter and the receiver are considered in this paper.

A. SI signal power analysis

According to wide-sense stationary uncorrelated scattering (WSSUS) model, $\forall l : h_{RSI,l}$ are assumed independent of each other, $\mathbb{E}[h_{RSI,l}] = 0$ and $\mathbb{E}\left[\left|h_{RSI,l}\right|^2\right] = \sigma^2_{RSI,l}$. $\mathbb{E}[.]$ indicates the statistical expectation operator. Furthermore, free-running oscillators (FRO) with Brownian motion process are used for generating the phase noise $[\phi[n+1] - \phi[n]] \sim \mathcal{N}(0, 4\pi\beta T_s)$, where $\phi[n]$ is Brownian motion with 3-dB bandwidth of β and T_s is the sample interval. Accordingly, after straight-forward manipulation, variance of the linear residual SI After ALC, $\sigma^{SI-ALC}_{k',m'} = \mathbb{E}\left[\left|R^{SI}_{k',m'}\right|^2\right]$, is derived as

$$\begin{aligned}\sigma^{SI-ALC}_{k',m'} = P_d \sum_{n_1=0}^{MK-1}\sum_{n_2=0}^{MK-1} f_{m'}[n_1] f^*_{m'}[n_2] e^{-4|n_1-n_2|\pi\beta T_s} \\ \left(\left|g_{TX,d} g_{RX,d}\right|^2 e^{\frac{j2\pi(n_1-n_2)\epsilon}{K}} + \left|g_{TX,I} g_{RX,I}\right|^2 e^{\frac{-j2\pi(n_1-n_2)\epsilon}{K}}\right) \\ \times \sum_{l=0}^{L-1}\sum_{k=0}^{K-1}\sum_{m=0}^{M-1} \sigma^2_{RSI,l} g_m[n_1-l] g^*_m[n_2-l] e^{\frac{j2\pi(n_1-n_2)(k-k')}{K}}.\end{aligned} \tag{10}$$

On the other hand, the power of the linear residual SI after C-DLC can be defined as $\sigma^{SI-DLC}_{k',m'} = \mathbb{E}\left[\left|R^{SI}_{k',m'} - R^{DLC}_{k',m'}\right|^2\right]$ which is given by

$$\begin{aligned}\sigma^{SI-DLC}_{k',m'} = P_d \sum_{n_1=0}^{MK-1}\sum_{n_2=0}^{MK-1} f_{m'}[n_1] f^*_{m'}[n_2] e^{-4|n_1-n_2|\pi\beta T_s} \\ \left(\left|g_{TX,d} g_{RX,d}\right|^2 e^{\frac{j2\pi(n_1-n_2)\epsilon}{K}} + \left|g_{TX,I} g_{RX,I}\right|^2 e^{\frac{-j2\pi(n_1-n_2)\epsilon}{K}}\right) \\ \times \sum_{l=0}^{L-1}\sum_{\substack{k=0 \\ k\neq k' \& m\neq m'}}^{K-1}\sum_{m=0}^{M-1} \sigma^2_{RSI,l} g_m[n_1-l] g^*_m[n_2-l] e^{\frac{j2\pi(n_1-n_2)(k-k')}{K}}.\end{aligned} \tag{11}$$

Note that (10) and (11) depend on multipath profile, 3-dB phase noise bandwidth, normalized CFO, IQ imbalance coefficients, number of subcarriers and time-slots and GFDM receiver and transmitter filters. Thus, all these parameters affect the efficiency of analog and digital SI cancellations. Similarly, the power of the conjugate residual SI after ALC and after C-DLC could be formulated as

$$\begin{aligned}\sigma^{SI-im-ALC}_{k',m'} = P_d \sum_{n_1=0}^{MK-1}\sum_{n_2=0}^{MK-1} f_{m'}[n_1] f^*_{m'}[n_2] e^{-4|n_1-n_2|\pi\beta T_s} \\ \left(\left|g_{TX,I} g_{RX,d}\right|^2 e^{\frac{j2\pi(n_1-n_2)\epsilon}{K}} + \left|g_{TX,d} g_{RX,I}\right|^2 e^{\frac{-j2\pi(n_1-n_2)\epsilon}{K}}\right) \\ \times \sum_{l=0}^{L-1}\sum_{k=0}^{K-1}\sum_{m=0}^{M-1} \sigma^2_{RSI,l} g^*_m[n_1-l] g_m[n_2-l] e^{\frac{-j2\pi(n_1-n_2)(k+k')}{K}}\end{aligned} \tag{12}$$

and

$$\begin{aligned}\sigma^{SI-im-DLC}_{k',m'} = P_d \sum_{n_1=0}^{MK-1}\sum_{n_2=0}^{MK-1} f_{m'}[n_1] f^*_{m'}[n_2] e^{-4|n_1-n_2|\pi\beta T_s} \\ \left(\left|g_{TX,I} g_{RX,d}\right|^2 e^{\frac{j2\pi(n_1-n_2)\epsilon}{K}} + \left|g_{TX,d} g_{RX,I}\right|^2 e^{\frac{-j2\pi(n_1-n_2)\epsilon}{K}}\right) \\ \times \sum_{l=0}^{L-1}\sum_{\substack{k=0 \\ k\neq k' \& m\neq m'}}^{K-1}\sum_{m=0}^{M-1} \sigma^2_{RSI,l} g^*_m[n_1-l] g_m[n_2-l] e^{\frac{-j2\pi(n_1-n_2)(k+k')}{K}}\end{aligned} \tag{13}$$

where $\sigma^{SI-im-ALC}_{k',m'} = \mathbb{E}\left[\left|R^{SI,im}_{k',m'}\right|^2\right]$ and $\sigma^{SI-im-DLC}_{k',m'} = \mathbb{E}\left[\left|R^{SI,im}_{k',m'} - R^{DLC,i}_{k',m'}\right|^2\right]$. Again, the results depend on the system parameters and the performance of the system can be evaluated for different configurations. Following (11) and (13), total power of residual SI signal after C-DLC may be expressed as

$$\sigma^{SI}_{k',m'} = \sigma^{SI-DLC}_{k',m'} + \sigma^{SI-im-DLC}_{k',m'}. \tag{14}$$

B. Desired signal power analysis

We assume that the desired signal is generated by (1) with i.i.d input symbols of $d^s_{k,m}$ with symbol energy p_d. No imperfections are considered in the transmitter of the desired signal. Thus, the desired symbol could be extracted from $R^s_{k',m'}$ as

$$d^{ss}_{k',m'} = d^s_{k',m'} \sum_{l=0}^{L-1}\sum_{n=0}^{MK-1} h^s_1[n,l] f_{m'}[n] g_{m'}[n-l] e^{\frac{-j2\pi k' l}{K}}. \tag{15}$$

Following the WSSUS model, $\forall l : h_{s,l}$ are assumed to be independent of each other, $\mathbb{E}[h_{s,l}] = 0$ and $\mathbb{E}\left[\left|h_{s,l}\right|^2\right] = \sigma^2_{s,l}$. Therefore, the variance of the desired symbol could be derived by

$$\sigma^s_{k',m'} = \mathbb{E}\left[\left|d^{ss}_{k',m'}\right|^2\right] = \left|g_{RX,d}\right|^2 P_d \sum_{l=0}^{L-1}\sum_{n_1=0}^{MK-1}\sum_{n_2=0}^{MK-1} \sigma^2_{s,l}$$
$$e^{-2|n_1-n_2|\pi\beta T_s} f_{m'}[n_1] f^*_{m'}[n_2] g_{m'}[n_1-l] g^*_{m'}[n_2-l] e^{\frac{j2\pi(n_1-n_2)\epsilon}{K}}. \tag{16}$$

According to the desired symbol, interference signals could be considered as $R^s_{k',m'} - d^{ss}_{k',m'}$ and $R^{s,im}_{k',m'}$. The variance of the first term could be calculated as $\sigma^{R^s}_{k',m'} - \sigma^s_{k',m'}$ where $\sigma^{R^s}_{k',m'} = \mathbb{E}\left[\left|R^s_{k',m'}\right|^2\right]$ is equal to

$$\sigma^{R^s}_{k',m'} = \left|g_{RX,d}\right|^2 P_d \sum_{l=0}^{L-1}\sum_{n_1=0}^{MK-1}\sum_{n_2=0}^{MK-1}\sum_{k=0}^{K-1}\sum_{m=0}^{M-1} \sigma^2_{s,l} e^{-2|n_1-n_2|\pi\beta T_s}$$
$$f_{m'}[n_1] f^*_{m'}[n_2] g_m[n_1-l] g^*_m[n_2-l] e^{\frac{j2\pi(n_1-n_2)(\epsilon+k-k')}{K}}. \tag{17}$$

Moreover, the variance of the second term could be expressed as

$$\sigma^{R^{s,im}}_{k',m'} = \left|g_{RX,I}\right|^2 P_d \sum_{l=0}^{L-1}\sum_{n_1=0}^{MK-1}\sum_{n_2=0}^{MK-1}\sum_{k=0}^{K-1}\sum_{m=0}^{M-1} \sigma^2_{s,l} e^{-2|n_1-n_2|\pi\beta T_s}$$
$$f_{m'}[n_1] f^*_{m'}[n_2] g^*_m[n_1-l] g_m[n_2-l] e^{\frac{-j2\pi(n_1-n_2)(\epsilon+k+k')}{K}}. \tag{18}$$

Thus, the total power of the interference signal is given by

$$\sigma^{s,i}_{k',m'} = \sigma^{R^s}_{k',m'} + \sigma^{R^{s,im}}_{k',m'} - \sigma^s_{k',m'}. \tag{19}$$

IV. SIR formulation and filter optimization

Herein, the SIR of the FD GFDM transceiver is derived and a receiver filter for maximizing the SIR is proposed. According to (14), (16) and (19), SIR of the estimated symbol in k'-th subcarrier and m'-th subsymbol may be expressed as

$$\Gamma_{k',m'} = \frac{\sigma^s_{k',m'}}{\sigma^{SI}_{k',m'} + \sigma^{s,i}_{k',m'}}. \tag{20}$$

Since GFDM use non-orthogonal subcarriers, it performs worse than OFDM in the presence of RF impairments. Thus, FD GFDM should achieve lower SIR than FD OFDM. However, GFDM contains degrees of freedom in receive filter design that can help us to improve the performance. To retain the benefits of GFDM such as lower out-of-band emissions, conventional filter is assumed for the transmitter side. On the other hand, the receiver filter is optimized to maximize the SIR. Let us denote $\mathbf{f_{k',m'}} = \mathbf{S}_{k'}\mathbf{M}_{m'M}\mathbf{f}_{0,0} \in \mathbb{C}^{MK\times 1}$ contains samples of $f_{k',m'}[n] = f_{m'}[n]e^{\frac{-j2\pi k' n}{K}}$ in (7) where $\mathbf{f}_{0,0} \in \mathbb{C}^{MK\times 1}$ is the column vector including receiver filter $f[n]$ samples, $\mathbf{M}_{m'M} \in \mathbb{C}^{MK\times MK}$ circularly shifts $\mathbf{f}_{0,0}$ and $\mathbf{S}_{k'} = \text{diag}\left(\left[1, e^{\frac{-j2\pi k'}{K}}, ..., e^{\frac{-j2\pi k'(MK-1)}{K}}\right]\right) \in \mathbb{C}^{MK\times MK}$ is the subcarrier mapping matrix. It is worth mentioning that (7) could be expressed as $\hat{d}^s_{k',m'} = \mathbf{y}_{IQ}\mathbf{f}_{k',m'}$ where $\mathbf{y}_{IQ} \in \mathbb{C}^{1\times MK}$ contains $y_{IQ}[n]$. Moreover, according to derivations, we rewrite the derived variances in matrix form as $\sigma^s_{k',m'} = \mathbf{f}^H_{k',m'}\mathbf{U}_{m'}\mathbf{f}_{k',m'}$, $\sigma^{SI}_{k',m'} = \mathbf{f}^H_{k',m'}\mathbf{V}^{SI}\mathbf{f}_{k',m'}$ and $\sigma^{s,i}_{k',m'} = \left(\mathbf{f}^H_{k',m'}\mathbf{V}^R\mathbf{f}_{k',m'} - \mathbf{f}^H_{k',m'}\mathbf{U}_{m'}\mathbf{f}_{k',m'}\right)$ where

$$U_{m'}[n_2,n_1] = \sum_{l=0}^{L-1} \left|g_{RX,d}\right|^2 P_d \sigma^2_{s,l} e^{-2|n_1-n_2|\pi\beta T_s} g_{m'}[n_1-l]$$
$$g^*_{m'}[n_2-l] e^{\frac{j2\pi(n_1-n_2)\epsilon}{K}}. \tag{21}$$

and

$$V^{SI}[n_2,n_1] = \sum_{l=0}^{L-1}\sum_{\substack{k=0\\k\neq k'}}^{K-1}\sum_{\substack{m=0\\m\neq m'}}^{M-1} P_d \sigma^2_{RSI,l} g_m[n_1-l] g^*_m[n_2-l]$$
$$e^{-4|n_1-n_2|\pi\beta T_s}\Big(\left|g_{TX,d}g_{RX,d}\right|^2 e^{\frac{j2\pi(n_1-n_2)(\epsilon+k)}{K}} + \left|g_{TX,I}g_{RX,I}\right|^2$$
$$e^{\frac{-j2\pi(n_1-n_2)(\epsilon-k)}{K}} + \left|g_{TX,I}g_{RX,d}\right|^2 e^{\frac{j2\pi(n_1-n_2)(\epsilon-k)}{K}} + \left|g_{TX,d}g_{RX,I}\right|^2$$
$$e^{\frac{-j2\pi(n_1-n_2)(\epsilon+k)}{K}}\Big). \tag{22}$$

and

$$V^R[n_2,n_1] = \sum_{l=0}^{L-1}\sum_{k=0}^{K-1}\sum_{m=0}^{M-1} P_d \sigma^2_{s,l} g_m[n_1-l] g^*_m[n_2-l]$$
$$e^{-2|n_1-n_2|\pi\beta T_s}\Big(\left|g_{RX,d}\right|^2 e^{\frac{j2\pi(n_1-n_2)(\epsilon+k)}{K}} + \left|g_{RX,I}\right|^2 e^{\frac{-j2\pi(n_1-n_2)(\epsilon+k)}{K}}\Big). \tag{23}$$

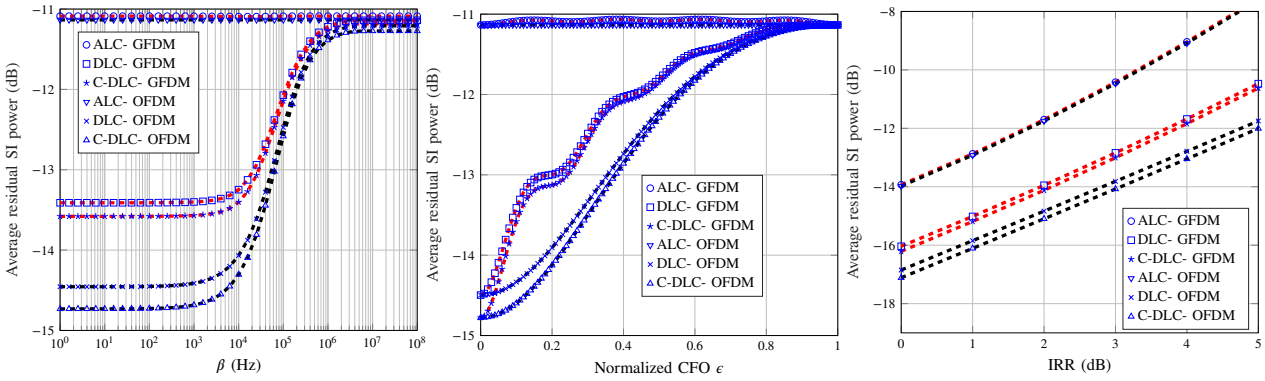

(a) (b) (c)

Fig. 2: Average residual SI power versus 3-dB phase noise bandwidth, normalized CFO and IRR.

Now, in order to find $\mathbf{f}_{0,0}$ that maximizes SIR, we rewrite SIR in matrix form as

$$\Gamma = \frac{\sum_{k'=0}^{K-1}\sum_{m'=0}^{M-1}\mathbf{f}_{k',m'}^{H}\mathbf{U}_{m'}\mathbf{f}_{k',m'}}{\sum_{k'=0}^{K-1}\sum_{m'=0}^{M-1}\mathbf{f}_{k',m'}^{H}\mathbf{V}\mathbf{f}_{k',m'} - \mathbf{f}_{k',m'}^{H}\mathbf{U}_{m'}\mathbf{f}_{k',m'}} = \frac{\mathbf{f}_{0,0}^{H}\mathbf{T}_1\mathbf{f}_{0,0}}{\mathbf{f}_{0,0}^{H}(\mathbf{T}_2-\mathbf{T}_1)\mathbf{f}_{0,0}} \tag{24}$$

where $\mathbf{V} = \mathbf{V}^{SI} + \mathbf{V}^{R}$, $\mathbf{T}_1 = \sum_{k'=0}^{K-1}\sum_{m'=0}^{M-1}\mathbf{M}_{m'M}^{H}\mathbf{S}_{k'}^{H}\mathbf{U}_{m'}\mathbf{S}_{k'}\mathbf{M}_{m'M}$ and $\mathbf{T}_2 = \sum_{k'=0}^{K-1}\sum_{m'=0}^{M-1}\mathbf{M}_{m'M}^{H}\mathbf{S}_{k'}^{H}\mathbf{V}\mathbf{S}_{k'}\mathbf{M}_{m'M}$. Therefore, the filter optimization problem for maximizing the SIR could be formulated as

$$\mathbf{f}_{0,0}^{opt} = \arg\max_{\mathbf{x}} \frac{\mathbf{x}^{H}\mathbf{T}_1\mathbf{x}}{\mathbf{x}^{H}(\mathbf{T}_2-\mathbf{T}_1)\mathbf{x}} \quad s.t. \quad ||\mathbf{x}||^2 = 1 \tag{25}$$

where $\mathbf{x} \in \mathbb{C}^{MK\times 1}$ and $||\mathbf{x}||$ indicates norm of $\mathbf{x}$. Optimal receiver filter is derived by the solution that is given by [18] as

$$\mathbf{f}_{0,0}^{opt} \propto \max\left[\text{eigenvector}\left((\mathbf{T}_2-\mathbf{T}_1)^{-1}\mathbf{T}_1\right)\right]. \tag{26}$$

Thus, we propose a receiver filter that maximizes the SIR of the FD GFDM under the RF impairments after ALC and C-DLC.

V. Simulation Results

In this section, the analytical derivations of residual SI signal power, intended signal power and SIR are verified with simulation results. Moreover, FD GFDM and FD OFDM are compared the presence of phase noise, CFO and IQ imbalance. Finally, we optimla receiver filter with conventional matched filter (MF) and zero forcing (ZF) receivers. The cyclic prefix for both OFDM and GFDM is equal to the length of the channel, and the number of subcarriers is 32. Additionally, GFDM uses M=5 time slots and root raised-cosine filter with the roll-off factor 0.1 and digital modulation 16-QAM (quadrature amplitude modulation). Sampling frequency is equal to 15.36 MHz [9]. Multipath Rayleigh fading channel with total of $L = 5$ taps is utilized for generating wireless channels. The power delay profile of SI channel is -30 dB, -65 dB, -70 dB and -75 dB for delays of 0, 1, 2 and 4 samples [9]. Furthermore, power delay profile of desired channel is $[-50, -75, -80, -85, -90]$ dBs. Same IQ imbalance level, $\text{IRR}_{Tx} = \text{IRR}_{Rx}$, is considered for the transmitter and the receiver. The theoretical results are shown with dash lines.

In Fig. 2, the residual SI power is plotted versus the 3-dB phase noise bandwidth, normalized CFO and IRR when ZF receiver is utilized for GFDM. For illustrating the impact of the conjugate residual SI cancellation, we consider both classical DLC (legend DLC) and C-DLC. As can be seen, the simulation results fully match the derived residual SI power. Moreover, C-DLC lowers SI power compared to DLC. Thus, cancelling the conjugate residual SI improves the performance significantly. In Fig. 2a, $\epsilon = 0.1$ and IRR = 2.5 dB, residual SI is plotted as a function of β. With increasing 3-dB phase noise bandwidth, post-DLC and post-C-DLC, average residual SI increases and saturates at a constant value that is lower than post-ALC residual SI. Furthermore, in Fig. 2b, $\beta = 10$ Hz and IRR = 2.5 dB and ϵ is changed. By increasing ϵ, average residual SI power after DLC boosts and approaches to average residual SI power after ALC. According to (10)-(13), 3-dB phase noise bandwidth, β, and normalized CFO, ϵ, appear in the exponential terms, and the trends in Fig. 2a and Fig. 2b for higher values of β and ϵ can be due to their appearance in the exponential function. The residual SI increases with IRR (Fig. 2c). In this figure, $\beta = 10$ Hz and $\epsilon = 0.1$ are fixed parameters and IRR is the independent variable. Finally, FD OFDM outperforms FD GFDM because of non-orthogonality of GFDM that generates more interference terms.

Fig. 3 depicts SIR as a function of 3-dB phase noise bandwidth, normalized CFO and IRR between FD GFDM with MF, ZF, proposed receiver filters and FD OFDM. Perfect match between the theoretical SIR (20) and numerical simulations can be observed. Moreover, FD OFDM achieves larger SIR than FD GFDM with conventional filters, emphasizing the necessity of designing an optimal receiver filter. Fig. 3a

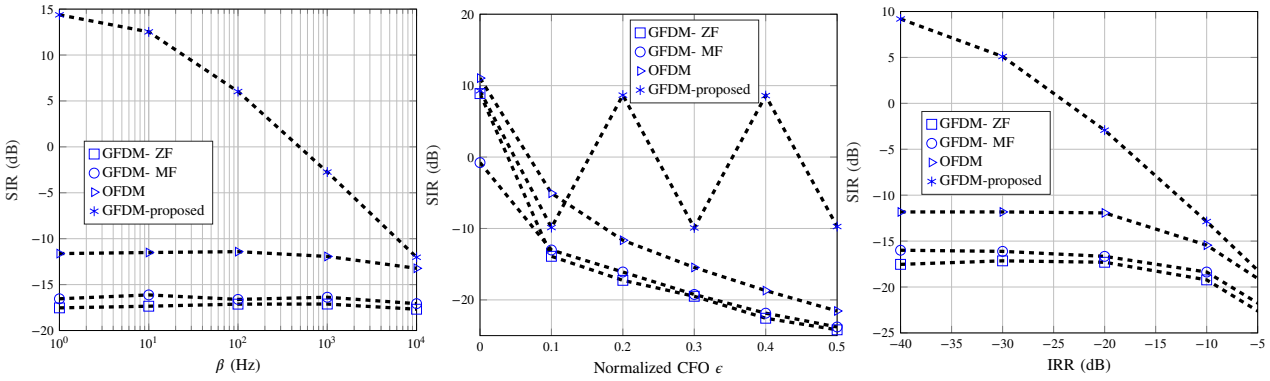

(a) (b) (c)

Fig. 3: SIR versus 3-dB phase noise bandwidth, normalized CFO and IRR.

illustrates SIR versus β when $\epsilon = 0.2$ and IRR $= -37.5$ dB. Obviously, by increasing β, SIR decreases in all cases. We can see that the SIR achieved by the optimized filter exceeds that of the others, e.g. in $\beta = 10$ Hz, SIR of the proposed filter is 25 dB higher than FD OFDM. Fig. 3b plots SIR as a function of ϵ when $\beta = 50$ Hz and IRR $= -37.5$ dB. In FD GFDM with conventional filters and OFDM, higher value of CFO, ϵ, lowers SIR, which is not surprising because frequency offset results in interference in general. Furthermore, the optimum filter with GFDM outperforms the other options, e.g. for $\epsilon = 0.2$, it achieves 20 dB higher SIR than FD OFDM. Fig. 3c represents the SIR versus IRR when $\beta = 50$ Hz and $\epsilon = 0.2$. In all cases, higher values of the IRR provides lower SIR. Furthermore, FD GFDM with the proposed filter is always better than FD OFDM, e.g. in IRR $= -30$ dB, the gap is 17 dB, indicating a significant improvement.

VI. Conclusion

In this paper, we investigated an FD GFDM transceiver in the presence of three RF impairments, namely phase noise, CFO and IQ imbalance. We considered both analog and digital SI cancellations and developed a complementary digital SI suppression method. Closed-form expressions for residual SI power and desired signal power were derived. The receiver filter for maximizing the SIR were proposed. Simulation results verified the analytical derivations. We observed that RF impairments degrade the SI cancellation methods. Moreover, the SIR results for FD GFDM with MF, ZF and proposed filter and FD OFDM show that proposed filter outperforms the other options. For instance, FD GFDM with the designed receiver filter achieves 25 dB higher SIR than FD OFDM when $\beta = 10$ Hz, $\epsilon = 0.2$ and IRR $= -37.5$ dB.

References

[1] IMT Vision, "Framework and overall objectives of the future development of IMT for 2020 and beyond," *International Telecommunication Union (ITU)*, 2015.

[2] D. Kim, H. Lee, and D. Hong, "A survey of in-band full-duplex transmission: From the perspective of PHY and MAC layers," *Commun. Surveys Tuts.*, vol. 17, no. 4, pp. 2017–2046, 2015.

[3] Z. Zhang, K. Long, A. V. Vasilakos, and L. Hanzo, "Full-duplex wireless communications: Challenges, solutions, and future research directions," *Proc. IEEE*, vol. 104, no. 7, pp. 1369–1409, 2016.

[4] M. Mohammadi, H. A. Suraweera, Y. Cao, I. Krikidis, and C. Tellambura, "Full-duplex radio for uplink/downlink wireless access with spatially random nodes," *IEEE Trans. Commun.*, vol. 63, no. 12, pp. 5250–5266, Dec 2015.

[5] M. Mohammadi, H. A. Suraweera, and C. Tellambura, "Uplink/downlink rate analysis and impact of power allocation for full-duplex cloud-RANs," *IEEE Trans. Wireless Commun.*, vol. 17, no. 9, pp. 5774–5788, Sep. 2018.

[6] N. Michailow and et.al., "Generalized frequency division multiplexing for 5th generation cellular networks," *IEEE Trans. Commun.*, vol. 62, no. 9, pp. 3045–3061, 2014.

[7] A. Mohammadian, A. Mohammadi, A. Abdipour, and M. Baghani, "Spectral analysis of GFDM modulated signal under nonlinear behavior of power amplifier," *arXiv:1803.02026 [eess.SP]*, 2018.

[8] C. D. Nwankwo, L. Zhang, A. Quddus, M. A. Imran, and R. Tafazolli, "A survey of self-interference management techniques for single frequency full duplex systems," *IEEE Access*, vol. 6, pp. 30242–30268, 2018.

[9] V. Syrjala, M. Valkama, L. Anttila, T. Riihonen, and D. Korpi, "Analysis of oscillator phase-noise effects on self-interference cancellation in full-duplex OFDM radio transceivers," *IEEE Trans. Wireless Commun.*, vol. 13, no. 6, pp. 2977–2990, 2014.

[10] D. Korpi, L. Anttila, V. Syrjälä, and M. Valkama, "Widely linear digital self-interference cancellation in direct-conversion full-duplex transceiver," *IEEE J. Sel. Areas Commun.*, vol. 32, no. 9, pp. 1674–1687, 2014.

[11] L. Samara et al., "Residual self-interference analysis for full-duplex OFDM transceivers under phase noise and I/Q imbalance," *IEEE Commun. Lett.*, vol. 21, no. 2, pp. 314–317, 2017.

[12] R. Li, A. Masmoudi, and T. Le-Ngoc, "Self-interference cancellation with nonlinearity and phase-noise suppression in full-duplex systems," *IEEE Trans. Veh. Technol.*, vol. 67, no. 3, pp. 2118–2129, 2018.

[13] B. Lim and Y. Ko, "SIR analysis of OFDM and GFDM waveforms with timing offset, CFO, and phase noise," *IEEE Trans. Wireless Commun.*, vol. 16, no. 10, pp. 6979–6990, 2017.

[14] S. Han, Y. Sung, and Y. H. Lee, "Filter design for generalized frequency-division multiplexing," *IEEE Trans. Signal Process.*, vol. 65, no. 7, pp. 1644–1659, 2017.

[15] A. Mohammadian, M. Baghani, and C. Tellambura, "Analysis and rate optimization of GFDM-based cognitive radios," *Trans. Emerg. Telecommunications Technol.*, vol. 29, no. 9, pp. e3435.

[16] A. Mohammadian, M. Baghani, and C. Tellambura, "Optimal power allocation of GFDM secondary links with power amplifier nonlinearity and ACI," *IEEE Wireless Commun. Lett.*, vol. 8, no. 1, pp. 93–96, 2019.

[17] W. Chung et al., "Interference cancellation architecture for full-duplex system with GFDM signaling," in *Signal Processing Conference (EUSIPCO)*, 2016, pp. 788–792.

[18] M. Sadek, A. Tarighat, and A. H. Sayed, "A leakage-based precoding scheme for downlink multi-user MIMO channels," *IEEE Trans. Wireless Commun.*, vol. 6, no. 5, pp. 1711–1721, 2007.